



Draft 1.1

Measurement of the Cross-section for Inclusive W Production in the Muon Channel at $\sqrt{s} = 1.96$ TeV Using the DØ Detector

The DØ Collaboration

(Dated: March 7, 2005)

A preliminary measurement of the cross-section for the process $p\bar{p} \rightarrow W \rightarrow \mu\nu$ at $\sqrt{s} = 1.96$ TeV is described. The measurement is performed using a data sample corresponding to an integrated luminosity of 96 pb^{-1} collected at the Fermilab Tevatron with the DØ experiment between February 2003 and September 2003. A total of 62,285 candidate events are observed, of which 7.8% are attributed to background processes. The result obtained is:

$$\sigma(p\bar{p} \rightarrow WX) \times \text{Br}(W \rightarrow \mu\nu) = 2989 \pm 15(\text{stat}) \pm 81(\text{syst}) \pm 194(\text{lumi}) \text{ pb.}$$

Preliminary Results for Winter 2005 Conferences

I. INTRODUCTION

A measurement of the cross-section for W boson production times the branching ratio for $W \rightarrow \mu\nu$ in $p\bar{p}$ collisions at 1.96 TeV is described below. This is done using 96 pb^{-1} of data collected by the DØ experiment. This process has become one of the ‘standard candles’ of hadron collider physics. It can be used to further understanding of the detector efficiencies and resolution, and can potentially be used to normalise other cross sections to. When combined with the $Z \rightarrow \mu^+\mu^-$ cross section it can be used to provide an indirect measurement of the width of the W boson.

The value of the cross section $p\bar{p} \rightarrow W \rightarrow \mu\nu$ is evaluated using the following formula:

$$\sigma(p\bar{p} \rightarrow WX) \times \text{Br}(W \rightarrow \mu\nu) = \frac{1}{\epsilon \times \mathcal{L}} \times \frac{N_{data}}{(1 + f_{bkg})} \quad (1)$$

where N_{data} is the number of candidate events, f_{bkg} is the fraction of these events attributed to background, ϵ is the efficiency of the selection cuts (the acceptance) and \mathcal{L} is the integrated luminosity of the sample [1]. The acceptance is evaluated using a parameterised simulation of the DØ detector with the tracking, muon identification and trigger efficiencies introduced from measurements made using data. The data sample is split into two separate sets due to different trigger configurations. The cross section $\sigma(p\bar{p} \rightarrow W \rightarrow \mu\nu)$ is evaluated separately for both of these sets which are combined for the final measurement.

II. THE DØ DETECTOR

The Run II DØ detector consists of the following main elements [2, 3]. A central-tracking system, consisting of a silicon microstrip tracker (SMT) and a central fiber tracker (CFT), both located within a 2 T superconducting solenoidal magnet. The SMT was designed to optimize tracking and vertexing within $|\eta| < 3$, where $\eta = -\ln(\tan(\frac{\theta}{2}))$. The system has a six-barrel longitudinal structure interspersed with 16 radial disks. The CFT has eight coaxial barrels, each supporting two doublets of overlapping scintillating fibers of 0.835 mm diameter, one doublet being parallel to the collision axis, and the other alternating by $\pm 3^\circ$ relative to the axis. Light signals are transferred via clear light fibers to solid-state photon counters (VLPC) that have $\approx 80\%$ quantum efficiency.

Central and forward preshower detectors located just outside of the magnet are constructed of several layers of scintillator strips. The next layer of detection involves three liquid-argon/uranium calorimeters: a central section (CC) covering $|\eta|$ up to ≈ 1 , and two end calorimeters (EC) extending coverage to $|\eta| \approx 4$.

A muon system resides beyond the calorimetry, and consists of a layer of tracking detectors and scintillation trigger counters before 1.8 T toroids, followed by two more similar layers after the toroids. Tracking at $|\eta| < 1$ relies on 10 cm wide drift tubes, while 1 cm mini-drift tubes are used at $1 < |\eta| < 2$. Coverage for muons is partially compromised, in the region of $|\eta| < 1.25$ and $4.25 < \phi < 5.15$ rad, by the calorimeter supports.

Luminosity is measured using plastic scintillator arrays located in front of the EC cryostats, covering $2.7 < |\eta| < 4.4$. The trigger and data acquisition systems are designed to accommodate the Run II luminosity. Based on preliminary information from tracking, calorimetry, and muon systems, the output of the first level of the trigger is used to limit the rate for accepted events to ≈ 1.5 kHz. At the next trigger stage, with more refined information, the rate is reduced further to ≈ 800 Hz. These first two levels of triggering rely on hardware and firmware. The third and final level of the trigger, with access to all the event information, uses software algorithms and a computing farm, and reduces the output rate to ≈ 50 Hz, which is written to tape.

DØ uses a right handed co-ordinate system, with the proton beam defining the positive z direction. The origin of the co-ordinate system is at the centre of the DØ detector, which roughly corresponds to the centre of the interaction region. The η co-ordinate is defined in two ways. Detector η relates to the position of the particle at a given layer of the detector, such as the start of the muon chambers or the edge of the CFT, and is measured with respect to (0,0,0). Physics η relates to the direction of travel and is measured with respect to the origin of the particle.

III. EVENT SELECTION CUTS: $W \rightarrow \mu\nu$ SIGNAL SAMPLE

The event selection requires evidence that a muon and a neutrino both with large momenta transverse to the beam axis are produced. Muons are identified by requiring a track in the muon system matched to a track in the central tracking system. The transverse momentum (p_T) of the muon is determined solely using the information from the central tracking system. The muon identification criteria require that the track in the muon system has scintillator and wire hits associated with it in both the layers within and without the toroid volume.

The muon is required to lie within the nominal geometrical acceptance of the muon chambers. This excludes the region where the beampipe enters the detector, delimited by $|x| < 110$ cm and $|y| < 110$ cm, where x and y are the ‘detector’ co-ordinates of a muon as it enters the muon system. The compromised region of the muon system containing the calorimeter supports defined by $4.25 < \phi < 5.15$ for $|\eta| < 1.25$ is also excluded. Unless otherwise stated the pseudo-rapidity, η , is measured at the position that the muons enter the muon system.

As the neutrino passes through the detector without interacting, its presence in an event has to be inferred by large missing transverse energy (\cancel{E}_T). To obtain the \cancel{E}_T , the vector sum of the energies, calculated from the angles of the energy deposited in the calorimeter, is corrected for the momentum of the muon. This vector is inverted to give the \cancel{E}_T .

The following additional selection criteria are applied:

1. The muon is required to have $p_T > 20$ GeV.
2. The event is required to have $\cancel{E}_T > 20$ GeV.
3. The transverse mass of the muon neutrino pair, M_T , is required to be greater than 40 GeV. The transverse mass is calculated as follows:

$$M_T = \sqrt{(\cancel{E}_T + p_T)^2 - (\cancel{E}_x + p_x)^2 - (\cancel{E}_y + p_y)^2}$$

where p_x and p_y are the components of the muon momentum in the x and y directions and \cancel{E}_x and \cancel{E}_y are the components of the \cancel{E}_T in the x and y directions. This cut removes the $b\bar{b}$ events where the muon and \cancel{E}_T lie close together in which the background fraction was found to be difficult to estimate.

4. To reduce the background from $b\bar{b}$ events where a b quark decays semi-leptonically into a muon, the muon is required to pass the following isolation cuts:
 - (a) $E_T^{\text{halo}} < (1.65 + 0.75 \times \mathcal{L}_I)$ GeV where $E_T^{\text{halo}} = \sum_{i, \Delta R=0.4} E_T^i - \sum_{i, \Delta R=0.4} E_T^i$ and \mathcal{L}_I is the instantaneous luminosity[?].
 - (b) $p_T^{\text{halo}} < (1.1 + 0.5 \times \mathcal{L}_I)$ GeV where $p_T^{\text{halo}} = \sum_{i, \Delta R=0.5} E_T^i$. In forming this sum, all tracks originating within 2 cm of the track matched to the muon in the z direction along the beam axis are considered and the track matched to the muon is excluded.
5. The central track matched to the muon is required to meet the following requirements:
 - (a) Must have at least one hit in the SMT associated with it.
 - (b) Must have a χ^2 per degree of freedom of the track fit of less than 3.3.

These requirements help minimise the contamination from mesons that decay in-flight (‘in-flight decays’).

6. To further remove in-flight decays and also cosmic rays, the $|dca|$ of the track associated with the muon is required to be less than 110 μm . The dca is the distance of closest approach of the muon track to the beam position in the x - y plane.
7. To reduce the background from $Z \rightarrow \mu^+\mu^-$ and cosmic rays, events are rejected if there is another muon in the event, passing the same quality requirements as the first muon. Events with a second central track with $p_T > 20$ GeV and $\Delta\phi > 2.1$ between the two tracks are also rejected. These are referred to as the ‘muon veto’ and the ‘track veto’ respectively.
8. The event is required to fire a single muon trigger. The data taking period is divided into those runs where the muon that fires the trigger can be anywhere in the muon chambers (set 1) and those where the muon that fires the trigger is constrained to lie with $|\eta| < 1.5$ (set 2). Apart from the constriction on the angular range in the second set the two triggers are identical.

For an event to pass the single muon trigger the muon must create hits in both the scintillation counters (the ‘L1 scint’ requirement) and the drift chambers (the ‘L1 wire’ requirement) identified at the first level of the trigger. The single muon trigger requires that the muon has a track reconstructed in the muon system, at the second level of the trigger, with a $p_T > 3$ GeV (the ‘L2M3’ requirement). The single muon trigger requires that the muon has a track reconstructed by the third level of the trigger system with a $p_T > 10$ GeV (the ‘L3TK’ requirement). In order to be able to evaluate the trigger efficiencies, the trigger objects are required to be spatially matched to the reconstructed muon.

After applying these selection cuts 62,285 candidate events are obtained in a sample with an integrated luminosity of 96 pb^{-1} .

Efficiency of	measured with respect to	set 1	set 2
reconstructed track		$0.834 \pm 0.004(\text{stat}) \pm 0.002(\text{sys})$	$0.834 \pm 0.004(\text{stat}) \pm 0.002(\text{sys})$
offline muon		$0.828 \pm 0.004(\text{stat}) \pm 0.002(\text{sys})$	$0.828 \pm 0.004(\text{stat}) \pm 0.002(\text{sys})$
‘L1 scint’(L1S)	offline muon (M)	0.917 ± 0.003	$0.761 \pm 0.005(\text{stat})$
‘L1 wires’(L1W)	M/L1S	0.974 ± 0.002	$0.807 \pm 0.005(\text{stat})$
‘L2M3’	M / L1S / L1W	0.984 ± 0.002	$0.984 \pm 0.002(\text{stat})$
‘L3TK’	track	0.792 ± 0.005	$0.792 \pm 0.005(\text{stat})$

TABLE I: Summary of average efficiencies.

IV. CALCULATION OF THE ACCEPTANCE

The acceptance(ϵ) in both of the data sets is evaluated using a parameterised simulation of the DØ detector. ϵ takes into account the geometrical acceptance of the muon chambers and the efficiency of the ‘kinematic’ cuts on p_T , E_T and M_T . ϵ also includes the isolation, trigger, tracking and muon identification efficiencies. The parameterised simulation uses events generated using the PYTHIA generator [4], using the CDF tune to the Z boson p_T [5], and employing the CTEQ6.1M PDF set [6].

The isolation, tracking, muon identification and trigger efficiencies are measured in data, as described below in Section IV A. Each efficiency is then introduced in the Monte Carlo by accepting a condition (e.g. has track, identified as muon, etc) with probability $P(\eta, \phi)$.

ϵ is defined to be the ratio between the number of events accepted to the number of events generated. Events are selected if they pass the event selection as described in Section III.

A. Measurement of Isolation, Tracking and Muon Efficiencies From Data

The isolation, tracking, muon identification and trigger efficiencies are all measured from the same data sample as the candidate events. This is done using the ‘tag and probe’ method, which uses the ability to select a clean sample of $Z \rightarrow \mu^+\mu^-$ events without requiring two isolated muons matched to tracks in the central detector [7]. An event is tagged as being $Z \rightarrow \mu^+\mu^-$ using all the requirements except the one being probed. For instance in the tracking efficiency measurement, a $Z \rightarrow \mu^+\mu^-$ event is tagged if there are two reconstructed muons, one of which is matched to a central track. The efficiency is defined as the fraction of the events in which the other muon has a track matched to it.

The muon identification and trigger efficiencies are measured in a similar way. Table I contains a summary of the average tracking, muon identification and trigger efficiencies. In order to properly account for geometrical correlations between these efficiencies they are measured as a function of position in the detector. These position-dependent efficiencies are simulated in the Monte Carlo used to evaluate the acceptance.

The systematic uncertainty on the tracking efficiency is due to a small bias introduced by the tag and probe method, caused by averaging over certain co-ordinates. Most of this bias can be removed by the correct choice of co-ordinate system. For instance the tracking efficiency is introduced as a function of η_{CFT} , where η_{CFT} is the η of the track as it leaves the central tracker, in bins of the z position of the origin of the muon track.

The size of this uncertainty is assessed using a GEANT [8] based simulation of the DØ detector. The efficiency evaluated using the tag and probe method is compared with that obtained using the Monte Carlo truth information. In both the tracking and muon identification efficiencies the efficiency obtained using the tag and probe method differs by 0.2% from that obtained using the Monte Carlo truth. These differences are assigned as systematic errors.

The isolation efficiency is also determined using the ‘tag and probe’ method using $Z \rightarrow \mu^+\mu^-$ data. The isolation is added into the Monte Carlo simulation as a fitted function of the p_T of the muon. The p_T dependence of the efficiency is expected to arise from the fact the the muon with higher p_T tends to travel in the same direction of the boson, hence in the opposite direction to any jet recoiling off the boson. As the parameters are determined using $Z \rightarrow \mu^+\mu^-$ data, the form is scaled down by a factor of the ratio of M_Z to M_W (0.882).

A comparison of the efficiency obtained using the tag and probe efficiency and the Monte Carlo truth information showed that requiring the control muon to be isolated introduces a 1% positive bias. If this requirement is not made, the efficiency sample will be contaminated with $b\bar{b}$ background, which has a lower isolation efficiency than $W \rightarrow \mu\nu$ or $Z \rightarrow \mu^+\mu^-$ events. As it is difficult in data to disentangle the effect of the bias and that of $b\bar{b}$ contamination the total efficiency is taken to be the average of that obtained without requiring the control muon to be isolated and that where the control muon is required to be isolated. The uncertainty on this is estimated to be half the size of the expected bias (0.5%).

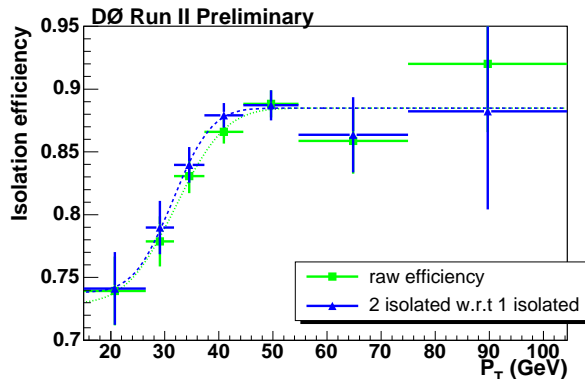


FIG. 1: Isolation efficiency as a function of the p_T of the central track evaluated using $Z \rightarrow \mu^+ \mu^-$ data. Dark line is where the control muon is required to be isolated and the light line is the case where no such requirement is made.

Source of Uncertainty	set 1	set 2	$\sqrt{(\text{covariance})}$
PDF	1.4%	1.2%	1.2%
Modelling of W p_T	0.2%	0.2%	0.2%
Statistical Uncertainty	0.9%	0.9%	0.9%
Isolation efficiency	0.9%	0.9%	0
Variation with time of the Efficiencies	0.6%	0.6%	0.6%
Modelling of z vertex	0.6%	0.8%	0.7%
'MIP' parameter	0.5%	0.5%	0.5%
E_T smearing parameters	0.3%	0.3%	0.3%
p_T scale	0.2%	0.2%	0.2%
Bias in muon identification efficiency	0.2%	0.2%	0.2%
Bias in tracking efficiency	0.2%	0.2%	0.2%
Total (excluding PDF)	1.7%	1.7%	1.5%
Total	2.1%	2.1%	1.9%

TABLE II: Summary of systematic uncertainties on the acceptance including uncertainties on the efficiencies.

After performing this procedure and scaling from the Z mass to the W mass the isolation efficiency was found to be

$$0.843 \pm 0.006(\text{stat}) \pm 0.005(\text{syst})$$

$$0.847 \pm 0.006(\text{stat}) \pm 0.005(\text{syst})$$

in data set 1 and set 2 respectively.

B. Acceptance and Associated Uncertainties

The acceptance in the first and second data sets are determined to be 0.216 and 0.189. A summary of the uncertainties on the acceptance is given in Table II.

The rest of this section consists of a brief description of each source of uncertainty and it's method of evaluation.

- The uncertainty on the acceptance due to the choice of PDF is evaluated using the method suggested by the CTEQ collaboration and the associated PDF sets [6].
- The uncertainty due to the modelling of the W boson p_T is obtained by comparing the acceptance above with the acceptance obtained using an alternative tune of PYTHIA [9].
- The statistical uncertainty is not due to the size of the Monte Carlo samples used to evaluate the acceptance, but rather due to the uncertainty on the input tracking, trigger and muon identification efficiencies. The accuracy

with which these efficiencies are known is determined from the data and the uncertainty is evaluated by varying each of the efficiencies when they are introduced into the simulation. Simultaneously the value of the efficiency in each bin is varied independently with a Gaussian distribution with sigma equal to the size of the uncertainty on that bin. This is done 400 times and the statistical uncertainty is given by the standard deviation of the ϵ values obtained.

- The uncertainty on the isolation due to biases in the tag and probe method and $b\bar{b}$ background in the efficiency sample is described in section IV A.
- The variation due to the time dependence of the efficiencies is found by evaluating the number of candidates, luminosity and efficiency in blocks of 5 pb^{-1} . The average cross section from this method is compared with the central value and the difference used to estimate the uncertainty due to the time dependence of the efficiencies.
- The luminous region as a function of z depends on the configuration of the beam, and so varies with time. The practice that has been adopted here is to tune the width and mean of the z distribution to agree with the average seen in data. The uncertainty in this tuning is propagated through to an uncertainty on the acceptance.
- The acceptance is evaluated using a parameterised model of the $D\bar{O}$ detector, which is tuned to data from $D\bar{O}$. These tunes have some uncertainty on them which results in uncertainties on the acceptance. The largest of these uncertainties (0.5%) arises from an uncertainty on the energy deposited by the muon in the calorimeter (the ‘MIP’ parameter). There are also non-negligible sources of uncertainty from the p_T scale of the tracker (0.2%) and in the parameterisation of the E_T (0.3%).
- There is an uncertainty on the both the tracking and muon identification efficiencies caused by a small bias in the ‘tag and probe’ method (see Section IV A).

V. BACKGROUND ESTIMATION

There have been four sources of background identified as contributing to the sample of candidate events, these are listed below:

1. The largest source of contamination is from the ‘electroweak’ background. This is caused by $Z/\gamma \rightarrow \mu^+\mu^-$ events, where only one of the muons is identified, and $W \rightarrow \tau\nu$ and $Z/\gamma \rightarrow \tau^+\tau^-$ events which produce one muon from tau decays. The size of this background is estimated with the Monte Carlo simulation used to evaluate the acceptance.
2. There is a contribution to the candidate events from events with quarks that decay semi-leptonically, producing muons (the ‘QCD’ Background).
3. A further source of contamination is from mesons, such as pions and kaons, that decay inside the tracking volume (‘In-flight decays’ or IFDs).
4. The last source of background is from cosmic rays.

The latter three backgrounds are all evaluated from data. The various contaminations are expressed as a fraction relative to the number of $W \rightarrow \mu\nu$ events.

A. The Electroweak Background

Samples of $Z/\gamma \rightarrow \mu^+\mu^-$ ($M_{\mu\mu} > 30 \text{ GeV}$), $W \rightarrow \tau\nu$ and $Z/\gamma \rightarrow \tau^+\tau^-$ are generated using the same Monte Carlo simulation used to evaluate the acceptance. The background is then the efficiency of the $W \rightarrow \mu\nu$ selection cuts applied to the particular background multiplied by the ratio of the background cross section with that of $W \rightarrow \mu\nu$. The cross section of $W \rightarrow \tau\nu$ is identical to that of $W \rightarrow \mu\nu$ and the ratio of $Z/\gamma \rightarrow \mu^+\mu^-$ ($M_{\mu\mu} > 30 \text{ GeV}$) to $W \rightarrow \mu\nu$ is taken to be 0.12 [10]. The contributions of all these backgrounds are listed in Table III. The uncertainty arises from the fact that the p_T scale of the isolation cut is not rescaled to either the higher scale of the Z or the lower one associated with the τ .

Background	set 1	set 2
$W \rightarrow \tau\nu$	0.025 ± 0.001	0.025 ± 0.001
$Z/\gamma \rightarrow \mu^+\mu^-$	0.043 ± 0.002	0.041 ± 0.002
$Z/\gamma \rightarrow \tau^+\tau^-$	0.0018 ± 0.0001	0.0017 ± 0.0001

TABLE III: Summary of electroweak backgrounds.

B. The QCD Background

The QCD background is evaluated from data using the matrix method. The matrix method uses a set of two simultaneous equations to extract the number of signal and background events in the sample.

Firstly the isolation cut, which has a high rejection factor for QCD background events, is removed. Then all other event selection requirements are applied, which results in a total of N events, of which B are background, and S are signal. Then the final event selection is applied, resulting in N_2 events. Two equations result:

$$N = B + S, \quad (2)$$

$$N_2 = fB + \epsilon S, \quad (3)$$

where f and ϵ are the efficiencies for background and signal events to pass the final event selection. Knowing the efficiencies f and ϵ , these equations can be solved to give the number of background events in the final sample:

$$B = \frac{\epsilon N - N_2}{\epsilon - f}. \quad (4)$$

To use the matrix method, the signal and background efficiencies have to be measured. This is done using as pure as possible samples of signal and background events. For the signal, efficiencies can be obtained in the data on samples of $Z \rightarrow \mu^+\mu^-$ events, which have a high purity. The background efficiency is obtained using muons with high \cancel{E}_T and low p_T . Fig. 2 shows the probability for single muons to pass the isolation cut as a function of p_T . The different bands are for for different \cancel{E}_T and M_T cuts. The efficiency for background events is taken from events with $\cancel{E}_T > 20$ GeV and $M_T > 40$ GeV in the low p_T region, where the probability for a single muon to be isolated is 0.06. In the high p_T region this sample becomes “contaminated” with $W \rightarrow \mu\nu$ events.

To extrapolate this efficiency into the high p_T signal region, like sign di-muon events, which tend to be predominantly $b\bar{b}$ events, are used. The probability for the muons in these events to be isolated shows no sign of increase with p_T . The different kinematics of these events means that we cannot use them to get an absolute value, but the general behaviour is assumed to be the same.

As it is impossible to extract the background efficiency in the signal region we take it to be 0.03 ± 0.03 , by halving the upper bound and quoting an uncertainty spreading from 0 to the upper bound.

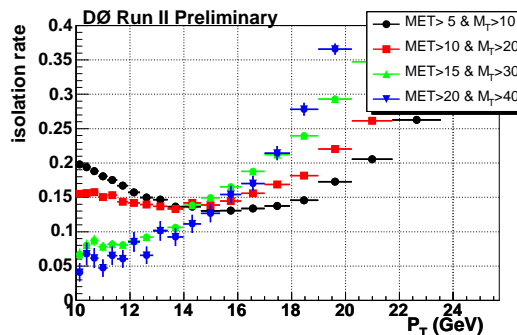


FIG. 2: Probability for a muon in a single muon event to be isolated as a function of p_T . The bands represent different cuts on \cancel{E}_T and M_T .

Using this figure for the background efficiency and that described in section IV A for the signal, the matrix method is used to evaluate the QCD background. Table IV summarises the numbers used to obtain the QCD background. The efficiency quoted for the signal is only an average. The actual calculation employs the p_T dependence discussed in Section IV A.

Quantity	set 1	set 2
N	41579	46777
N_2	29159	33126
fB	228	238
ϵ	0.843 ± 0.008	0.847 ± 0.008
f	0.03 ± 0.03	0.03 ± 0.03
f_{QCD}	0.008 ± 0.008	0.007 ± 0.007

TABLE IV: Numbers used to calculate QCD background with the Matrix Method.

C. Muons From In-Flight Meson Decays and Cosmic Rays Backgrounds

Mesons, such as kaons and pions, can decay to muons before showering in the calorimeter. This can produce an isolated muon in the muon chambers in association with a track in the central detector, faking a $W \rightarrow \mu\nu$ event. Trying to fit a single track from the combination of the meson and the muon tracks tends to produce a larger χ^2 in the track fit and a poorer dca and p_T resolution. Combining this poor p_T resolution with the fact that the muon produced in the decay tends to have lower p_T results in a discrepancy between the p_T as measured by the muon system and that as measured by the central tracker.

Cosmic rays can pass the $W \rightarrow \mu\nu$ event selection if they are reconstructed in both the muon system and the tracker. As they are not produced in the interaction point, they tend to have large values of dca . It is the dca distribution that is used to discriminate the signal events from these backgrounds. The procedure adopted is to create template dca distributions for signal and these backgrounds. The dca distribution in the candidate events is then fitted with a sum of these templates to estimate the fraction of candidates that are due to ‘in-flight decay’ and cosmic backgrounds.

The template for the signal is taken from $Z \rightarrow \mu^+\mu^-$ events which are assumed to be pure. The template distributions for the ‘in-flight decay and cosmic ray backgrounds are taken from samples enhanced in the relevant background. The dca distribution of the candidate events is fitted using the three templates to obtain the fraction of events attributed to signal and backgrounds.

Following this procedure the background from cosmic rays is found to be negligible and that from in-flight decays found to be (0.0022 ± 0.0012) . The uncertainty on this number is a systematic error obtained by varying the sample on which the template for the ‘in-flight decay’ background is fitted from.

VI. RESULTS

A. Comparison between Data and Monte Carlo and Cross Checks

In order to demonstrate that the Monte Carlo simulation provides a realistic description of the data a series of comparison plots are included. In each of the comparison plots the data is shown as points with error bars, the signal Monte Carlo is shown as a solid X coloured histogram, the QCD background is shown as a solid black histogram and the electroweak background is shown as other solid histograms. In each plot the Monte Carlo has been normalised to the number of events in data.

Figure 3 shows the p_T distribution of the muon for the candidate data events for both sets combined. The plot is displayed in two forms: the left plot on a linear and the right plot on a logarithmic scale.

Figure 4 shows the E_T distribution of the muon for the candidate data events for both sets combined. The plot is displayed in two forms: the left plot on a linear and the right plot on a logarithmic scale.

Figure 5 shows the M_T distribution of the muon for the candidate data events for both sets combined. The plot is displayed in two forms: the left plot on a linear and the right plot on a logarithmic scale.

Figure 7 shows the η distribution of the muon for the candidate data events for both sets combined. The left plot shows this in the first set and the right plot in the second.

Figure 6 shows the ϕ distribution of the muon for the candidate data events for both sets. The left plot shows this in the first set and the right plot in the second.

There are also several cross checks performed. The cross section is evaluated separately in the forward and central regions and found to be relatively stable. The E_T and p_T cuts are varied. The cross section is stable in data set 1, but in data set 2 tightening the kinematic cuts produces a 2.5% decrease in the cross section, which is quoted as a systematic. The ‘track veto’ and the ‘muon veto’ are each removed separately, each resulting in a 1.5% change in the cross section, which is quoted as a systematic.

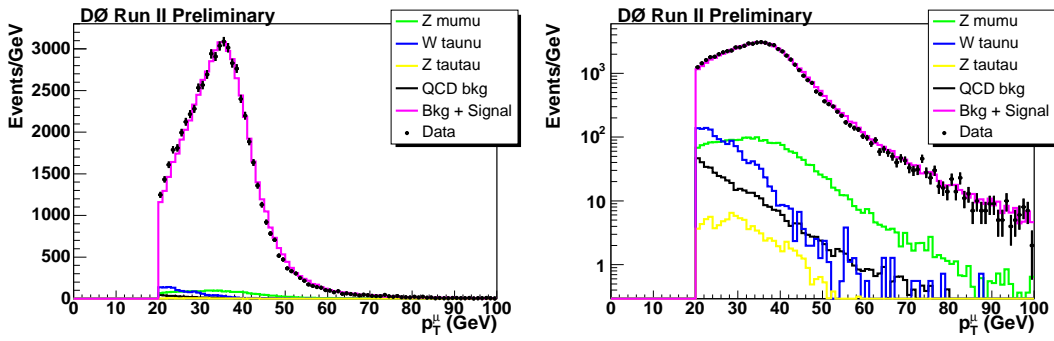


FIG. 3: Comparison of the p_T distribution in the data (dots) and the Monte Carlo prediction. This is shown on both linear (left plot) and logarithmic scales (right plot).

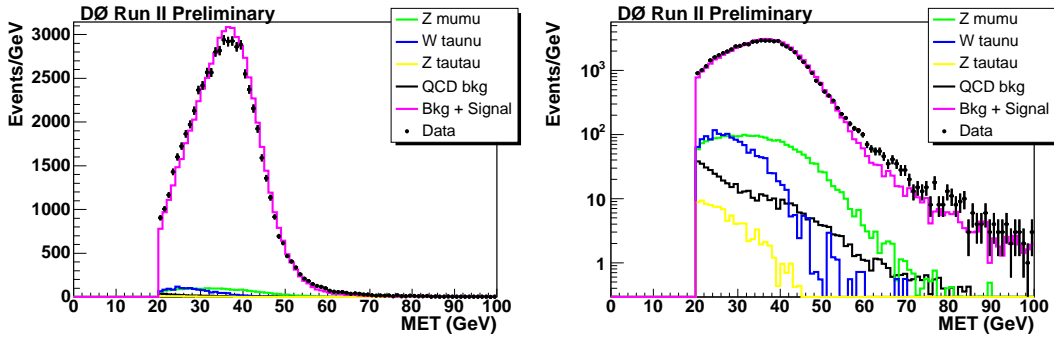


FIG. 4: Comparison of the E_T distribution in the data (dots) and the Monte Carlo prediction. This is shown on both linear (left plot) and logarithmic scales (right plot).

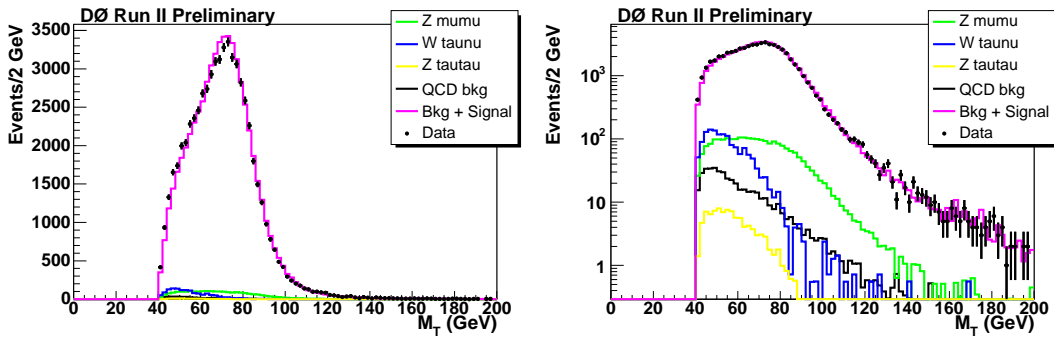


FIG. 5: Comparison of the M_T distribution in the data (dots) and the Monte Carlo prediction. This is shown on both linear (left plot) and logarithmic scales (right plot).

B. Cross Section Computation

The inclusive $W \rightarrow \mu\nu$ production cross section is calculated using equation (1). The values of the variables used to evaluate the cross section in the two sets are given in Table V.

In Table VI we summarise the different fractional contributions to the uncertainty of the cross section measurement. In the second data set the following result is obtained:

$$\sigma(pp\bar{p} \rightarrow WX) \times \text{Br}(W \rightarrow \mu\nu) = 3020 \pm 16(\text{stat}) \pm 114(\text{syst}) \pm 196(\text{lumi}) \text{ pb.}$$

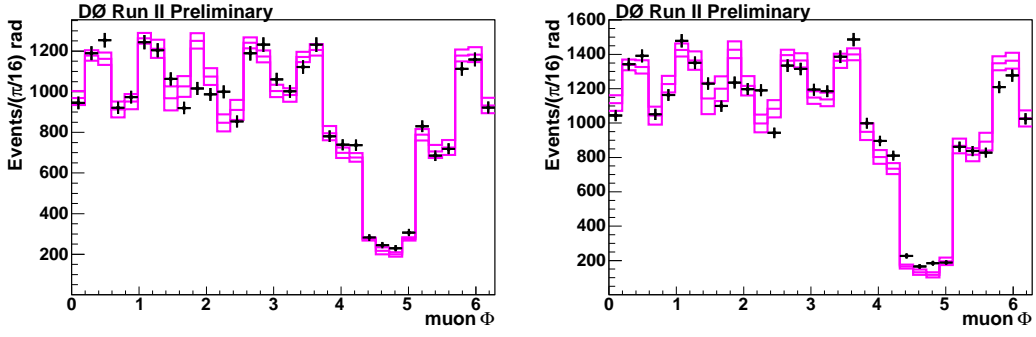


FIG. 6: Comparison of the ϕ distribution of the muon in the data (dots) and the Monte Carlo prediction. This is shown for both the first (left plot) and second sets (right plot). The bands in the MC histograms are due to the statistical uncertainty on the input efficiencies.

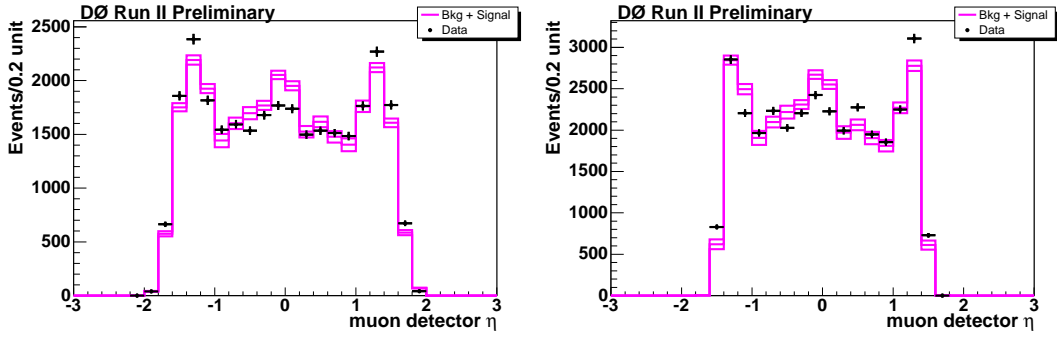


FIG. 7: Comparison of the η distribution of the muon in the data (dots) and the Monte Carlo prediction. This is shown for both the first (left plot) and second sets (right plot). The bands in the MC histograms are due to the statistical uncertainty on the input efficiencies.

In the first data set the following result is obtained:

$$\sigma(p\bar{p} \rightarrow WX) \times \text{Br}(W \rightarrow \mu\nu) = 2984 \pm 17(\text{stat}) \pm 81(\text{syst}) \pm 194(\text{lumi}) \text{ pb.}$$

C. Summary

Combining these results, weighting them by their uncorrelated uncertainty, gives a final cross section of

$$\sigma(p\bar{p} \rightarrow WX) \times \text{Br}(W \rightarrow \mu\nu) = 2989 \pm 15(\text{stat}) \pm 81(\text{syst}) \pm 194(\text{lumi}) \text{ pb.}$$

Figure 8 shows the theoretical prediction [11] of $\sigma(p\bar{p} \rightarrow WX) \times \text{Br}(W \rightarrow \mu\nu)$ for $p\bar{p} \rightarrow XW \rightarrow X + l\nu$ as a function of centre of mass energy with the measurements made by D0 and CDF [12] in the electron and muon channels. It

Sample	set 2	set 1
Number of candidates	33126	29159
Acceptance and efficiencies	18.9 %	21.6%
Electroweak background	6.7%	7.0%
IFD and cosmic background	0.25 %	0.25%
QCD background	0.7 %	0.8 %
Luminosity	53.7 pb ⁻¹	41.9 pb ⁻¹
Cross section	3020 pb	2984 pb

TABLE V: Summary of figures used to evaluate the results in the two data sets.

Source of uncertainty	set 2	set 1	$\sqrt{\text{covariance}}$
statistical	0.6%	0.6%	0
acceptance and efficiencies (exc PDF)	1.7%	1.7%	1.5×10^{-2}
QCD background	0.7%	0.8%	0.8×10^{-2}
Electroweak background	0.4%	0.4%	0.4×10^{-2}
PDF uncertainty	0.9%	0.8%	0.9×10^{-2}
Choice of Veto	1.5%	1.5%	1.5×10^{-2}
Variation with Kinematic Cuts	2.5%	0.0%	0.
Total relative uncertainty	3.8%	2.8%	2.7×10^{-2}

TABLE VI: Summary of the fractional uncertainties in the first and second sets. The third column is the co-variance. To be conservative most quantities are assumed to be completely correlated.

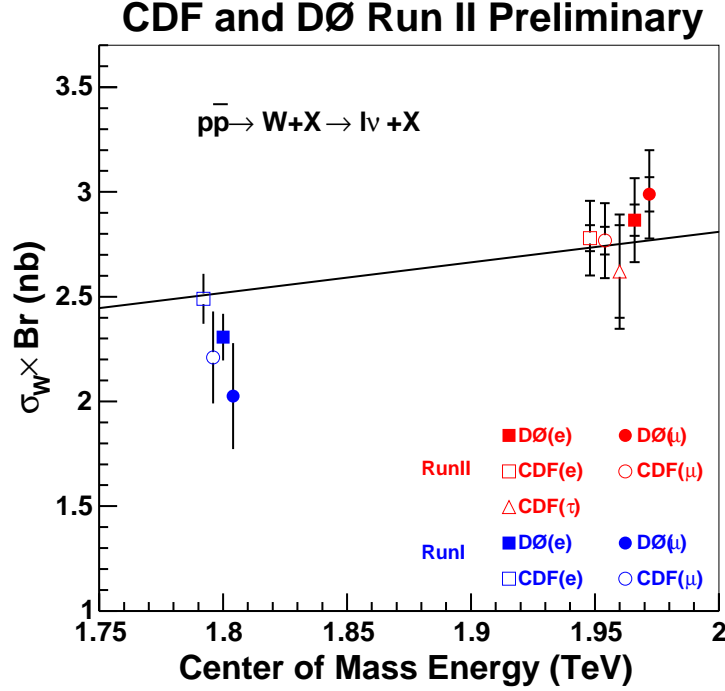


FIG. 8: The theoretical prediction of $\sigma(p\bar{p} \rightarrow WX) \times \text{Br}(W \rightarrow \mu\nu)$ for $p\bar{p} \rightarrow XW \rightarrow X + l\nu$ as a function of the centre of mass energy as predicted by Matsuura and van Neerven [11]. The experimental measurements in the muon and electron channels for the DØ and CDF [12] experiments are shown as points with error bars. Note that all the Run II measurements are made at 1.96 TeV. They are spaced out along the x axis to aid the viewer.

can be seen that the result is in agreement with the theoretical prediction, as well as the same measurement at DØ in the electron channel [13], and measurements at CDF in the muon, τ lepton and electron channels [12].

-
- [1] T. Edwards *et al.*, DØ Note **4328** (2003).
 - [2] S. Abachi, *et al.*, Nucl. Instrum. Methods Phys. Res. A **338**, 185 (1994).
 - [3] V. Abazov, *et al.*, in preparation for submission to Nucl. Instrum. Methods Phys. Res. A, and T. LeCompte and H.T. Diehl, “The CDF and DØ Upgrades for Run II”, Ann. Rev. Nucl. Part. Sci. **50**, 71 (2000).
 - [4] T. Sjöstrand *et al.* Computer Physics Commun. **135**, 238 (2001).
 - [5] U. Yang and Y. Kim, ‘ISR Studies on Drell-Yan’, Fermilab MC Workshop (2003) <http://cepa.fnal.gov/patriot/mc4run2/MCTuning/031204/unki.pdf>.
 - [6] J. Pumplin *et al.*, J.H.E.P. **310** 046 (2003).
 - [7] E. Nurse and P. Telford, DØ Note **4573** (2004).
 - [8] R. Brun *et al.* CERN-DD-78-2-REV.

- [9] B. Tiller and T. Nunneman, DØ Note **4660** (2004).
- [10] S. Frixione and B.R. Weber, J.H.E.P. **206** 029 (2002).
S. Frixione, P. Nason and B.R. Weber, J.H.E.P. **308** 007 (2003).
- [11] C.R. Hamberg, W.L. van Neerven and T. Matsuura, Nucl. Phys. **B359**, 343 (1991).
- [12] D. Acosta *et al*, submitted to P. R. L. (hep-ex/0406078) (2004).
- [13] D. Chapin *et al*, DØ Note **4403** (2004).
□ A typical value in our sample is $\mathcal{L}_{\mathcal{I}} = 0.6 \times 10^{30} \text{cm}^{-2} \text{s}^{-1}$. per crossing (in units of $10^{30} \text{cm}^{-2} \text{s}^{-1}$)